

**Application of the matrix-effective-potential formalism
to electron-neon scattering at 150–700-eV impact energy and
comparison to optical-potential calculations**

Devarajan Thirumalai and Donald G. Truhlar

*Department of Chemistry and Chemical Physics Program, University of Minnesota,
Minneapolis, Minnesota 55455*

(Received 20 October 1981)

We apply two methods to predict integral and differential elastic and absorption cross sections for electron-neon scattering at 150–700 eV: a matrix-effective-potential (MEP) formalism and an optical-potential formalism. For the optical potential we use the absorption potential that Green, Rio, and Ueda adjusted to give accurate absorption cross sections, and we show that the real part of the potential can be chosen so that the calculated elastic-scattering cross sections also agree with experiment. The MEP model, with no parameters adjusted to experiment, is even more successful. The agreement with available experimental elastic differential cross sections is better than 10% in many cases and is about 40% at worst; agreement with experimental total inelastic cross sections averages 3% at four energies. An interesting conclusion from the optical-potential calculations is that when the absorption potential is included in the optical potential, accurate elastic cross sections can be calculated even at high energy by using an *adiabatic* polarization potential.

I. INTRODUCTION

The inclusion of the dynamic effects of charge polarization is the most difficult part in quantum-mechanical calculations of electron-atom and electron-molecule scattering.¹ There are several models that take into account the polarization effect. The adiabatic polarization potential (APP) takes into account the complete response of the target to the presence of a stationary electron.² Since, however, the atom or molecule does not have infinite time to respond to the incident electron, the true effect of charge polarization on the interaction potential is always less than that predicted by the adiabatic model. Furthermore, the polarization effect should decrease as the interaction time decreases, so any realistic incorporation of charge polarization in the effective potential should be explicitly energy dependent. Another method to include nonadiabatic polarization effects in the treatment of electron collisions makes use of matrix-effective potentials, and it has been shown that with matrix-effective potentials the nonadiabatic polarization effects can be simulated by energy-independent local potentials.^{3,4} In this paper we use this approach to calculate integral and differential cross sections for elastic scattering and total (elastic and inelastic plus ionization)

scattering cross sections for electron-neon scattering.

The matrix-effective-potential (MEP) method was first proposed in a version based on perturbation-theory adiabatic polarization potentials, and it was applied successfully to electron-helium scattering at impact energies in the range 30–400 eV.^{3,4} In a later paper we considered a version of the MEP based on variational adiabatic polarization potentials,⁵ and in this paper we apply this MEP method to electron-neon scattering at impact energies in the range 150–700 eV. In the MEP method, the matrix potential is determined so that it takes into account the full target response at r (r being the distance of the incident electron from the origin at the center of mass of the target) in the adiabatic limit and goes to the static-exchange limit in the decoupling limit. In the previous study of electron-helium scattering an APP determined using second-order perturbation theory⁶ was used to obtain the MEP, whereas the APP used in the present study is a variational one.⁷ In our previous study of both versions of the MEP method we suggested two- and three-channel implementations.⁵ However in the present study we consider only the two-channel one.

Another approach to treating charge polarization is the use of phenomenological complex optical po-

tentials. For such potentials the imaginary part of the potential causes a loss of flux from the incident channel and plays a comparable role to the pseudo-channel of the MEP. This sort of approach is a reasonable way to analyze experimental data; it has been used very widely in nuclear physics and more recently it has also been applied to electron-atom scattering. For comparison with the MEP approach we present calculations employing the phenomenological form of the imaginary part of the optical potential suggested by Green *et al.*⁸ The results of the two approaches will be compared to each other and also to recent experimental and other theoretical results.

We use hartree atomic units throughout this paper. The unit of energy is the hartree (E_h); distance is measured in units of bohrs (a_0); the mass is in units of mass of an electron; and angular momentum and action are in units of \hbar .

II. THEORY

The general approach of the coupled-channel formalism involves expanding the total scattering wave function of the target plus the incident electron in terms of angular functions for the orientation of the incident electron and either eigenfunctions of the target or some suitable pseudostates, i.e.,¹

$$\psi(\vec{r}, \vec{x}) = \sum_{i=1}^M \mathcal{A} f_i(r) Y_{l_i m_i}(\hat{r}) \phi_i(\vec{x}), \quad (1)$$

where \vec{r} denotes the coordinate of the incident electron, \vec{x} denotes collectively the coordinates of the target electrons, and \mathcal{A} is an antisymmetrizer; $\phi_i(\vec{x})$ stands for either a target eigenfunction or a pseudostate; and $f_i(r)$ is a radial wave function of the scattering electron. The specification of l_i and m_i for each i depends on the details of the chosen basis set; these details are not needed for the present discussion. The well-known variational equations for the radial function are

$$\left[\frac{d^2}{dr^2} - \frac{l_i(l_i+1)}{r^2} + k_i^2 \right] f_i(r) = 2 \sum_{j=1}^M V_{ij} f_j(r), \quad (2)$$

where, because of \mathcal{A} , V_{ij} is a nonlocal operator. In Eq. (2) the wave number k_i in channel i is related to the total energy E and the internal energy ϵ_i of channel i by

$$k_i^2 = 2(E - \epsilon_i). \quad (3)$$

We choose the zero of energy so that $\epsilon_1 = 0$. Such a calculation takes into account all the dynamic charge-polarization effects within the chosen M -channel basis to all orders. However, in some cases M must be very large to yield convergence. The MEP method used here involves a two-channel effective representation of the scattering problem, i.e., we set $M = 2$ and replace the actual potential matrix $V(r)$ by an effective one $V^{\text{MEP}}(r)$, such that the elements of the 2×2 effective-potential matrix $V^{\text{MEP}}(r)$ are local. (In principle one could retain a nonlocal description of the static-exchange effects but still reduce the $M \times M$ matrix of nonlocal operators to a 2×2 one as a way to simplify the treatment of charge polarization. In our work, however, we have only examined approximations in which the matrix-effective potential is local.) For the diagonal elements $V_{ii}^{\text{MEP}}(r)$ we use the sum $V^{\text{SE}}(r, E)$ of the ground-state static potential⁹ $V^{\text{S}}(r)$ and a local approximation¹⁰ $V^{\text{E}}(r, E)$ for exchange. We make the centrifugal sudden approximation¹¹

$$l_2 = l_1 \quad (4a)$$

and we set

$$k_2^2 = k_1^2 - 2\omega, \quad (4b)$$

where ω is an average excitation energy. We require $V_{21}^{\text{MEP}}(r) = V_{12}^{\text{MEP}}(r)$ so that $V^{\text{MEP}}(r)$ is Hermitian. Then the quantities that need be specified to construct $V^{\text{MEP}}(r)$ are $V_{12}(r)$ and ω . We choose ω equal to an effective-excitation energy as discussed in the Appendix, and we determine $V_{12}^{\text{MEP}}(r)$ so that the adiabatic potential implicit in $V^{\text{MEP}}(r)$ is equal to the variationally calculated adiabatic polarization potential $V^{\text{Pa}}(r)$. This gives

$$\det \begin{bmatrix} -V^{\text{Pa}}(r) & V_{12}^{\text{MEP}}(r) \\ V_{12}^{\text{MEP}}(r) & \omega - V^{\text{Pa}}(r) \end{bmatrix} = 0. \quad (5)$$

Solving Eq. (5) for $V_{12}^{\text{MEP}}(r)$ yields

$$V_{12}^{\text{MEP}}(r) = \{ [V^{\text{Pa}}(r)]^2 - \omega V^{\text{Pa}}(r) \}^{1/2}. \quad (6)$$

This completes the prescription for $V^{\text{MEP}}(r)$ and reduces the dynamics to an effective two-channel problem.

Notice that both terms in the radicand in Eq. (6) are positive and that Eq. (6) reduces in the perturbative limit to the result that has been previously used,^{3,4} i.e.,

$$V_{12}^{\text{MEP}}(r) \sim [-\omega V^{\text{Pa}}(r)]^{1/2}. \quad (7)$$

This limit applies at large r where $V^{\text{Pa}}(r)$ is small.

As an alternative to the MEP method we consid-

er the method of complex single-channel optical potentials. Although formal prescriptions exist for the *ab initio* determination of the exact optical potential, these are too difficult to apply. Thus the customary procedure is to assume a reasonable (physically based) form with adjustable parameters for the optical potential and subsequently to tune these parameters to yield correct observables. Unfortunately there is no general theoretical justification for any particular parametrized form for the optical potential. Thus empirical tests and comparisons are very useful. Here we use the energy-dependent functional form suggested by Green *et al.*⁸:

$$V^A(r, E) = -W_0(E) \left[\frac{e^{-r/d}}{r} - \frac{e^{-r/s}}{r} \right], \quad (8)$$

where the r dependence in Eq. (8) was chosen by Green *et al.* by analogy to the static potential. They obtained a functional form for $W_0(E)$ by imposing two constraints: (a) $W_0(E)$ should be zero below the threshold of the atom, and (b) it is assumed that asymptotically $W_0(E)$ should go over to the form of high-energy inelastic cross sections, i.e.,

$$W_0(E) \underset{E \rightarrow \infty}{\sim} E^{-1} \ln E.$$

Based on these constraints they postulated the form

$$W_0(E) = w \frac{\epsilon_2}{E} \ln \left[\beta \left[\frac{E}{\epsilon_2} - 1 \right]^\nu + 1 \right], \quad (9)$$

where ϵ_2 is the lowest electronic excitation energy, and w , β , and ν are adjustable parameters. Green *et al.*⁸ adjusted these parameters so that their calculations reproduced the experimental absorption cross sections as well as possible. The actual values of the parameters appearing in $V^A(r, E)$ and $W_0(E)$ are given in Table I.

TABLE I. Values of parameters used in the absorption potential of Green *et al.*

Parameter	Value (a.u.)
d	$1.841a_0$
s	$3.292a_0$
w	$42.72E_h$
ν	1.872
β	0.01108
ϵ_2	$0.62E_h$

III. CALCULATIONS

As explained in Sec. II, $V_{ii}^{\text{MEP}}(r)$ is set equal to the sum $V^{\text{SE}}(r, E)$ of the static and exchange potentials for the ground state of the target. The static potential is evaluated from the analytic fit of Strand and Bonham,⁹ based on the Hartree-Fock results of Roothaan *et al.*¹² The exchange potential is evaluated using the semiclassical exchange approximation,¹⁰ which makes it a functional of the static potential and the target density. The latter was also taken from the compilation of Strand and Bonham.⁹ The APP used in the calculations was obtained from *ab initio* extended-basis-set perturbed-Hartree-Fock variational calculations described elsewhere.⁷ At large r the APP was fit to

$$V^{\text{Pa}}(r) \sim \frac{\alpha_0}{2r^4} - \frac{c}{r^6}, \quad (10)$$

where α_0 is the dipole polarizability. The basis set used in Ref. 7 gives the following value for α_0 ; it equals $2.359a_0^3$.

Notice that the MEP model tacitly includes the parameter ω . We showed in Ref. 4 that the results are not overly sensitive to this parameter. In the present work we chose ω without reference to experimental data by the method discussed in the Appendix. Other choices are of course possible, but the choice in the Appendix is the only one we tried.

For comparison purposes we also made calculations using a complex one-channel potential with the imaginary part equal to the phenomenological absorption potential $V^A(r, E)$ of Green *et al.*,⁸ as summarized above. For these calculations we tried three different forms of the real part of the optical potential. In the original calculations of Green *et al.*⁸ the real part of the optical potential was represented by an approximate static-exchange potential; thus the first potential we try is

$$V^{\text{SEA}}(r, E) = V^{\text{SE}}(r, E) + iV^A(r, E). \quad (11)$$

We also tried

$$V^{\text{SEPaA}}(r, E) = V^{\text{SEPa}}(r, E) + iV^A(r, E),$$

where

$$V^{\text{SEPa}}(r, E) = V^{\text{SE}}(r, E) + V^{\text{Pa}}(r). \quad (12)$$

This includes the effects by virtual charge polarization by including the APP in the real part of the optical potential. As mentioned in the introduction, however, the polarization potential should be

nonadiabatic (abbreviated na) and energy dependent. Thus we also tried

$$V^{\text{SEPnaA}}(r, E) = V^{\text{SE}}(r, E) + V^{\text{Pna}}(r, E) + iV^{\text{A}}(r, E), \quad (13)$$

where $V^{\text{Pna}}(r, E)$ is the energy-dependent polarization potential of Ref. 4, i.e.,

$$V^{\text{Pna}}(r, E) = V^{\text{Pa}}(r) / (1 + 12E / \omega^2 r^2), \quad (14)$$

where ω is determined by the method described in the Appendix. Some of the components of these optical potentials are illustrated in Fig. 1.

In the MEP method the two-channel real Schrödinger equation was solved by our variable-step-size Numerov program.¹³ For the optical-potential calculations the complex single-channel Schrödinger equation was solved by integrating the phase equation¹⁴ using a variable-step-size fourth-order Runge-Kutta integration procedure. For both sets of calculations, the resulting phase shifts are complex, i.e.,

$$\eta_l = \delta_l + i\gamma_l. \quad (15)$$

The physical observables are calculated from these complex phase shifts by the standard formulas^{15,16}

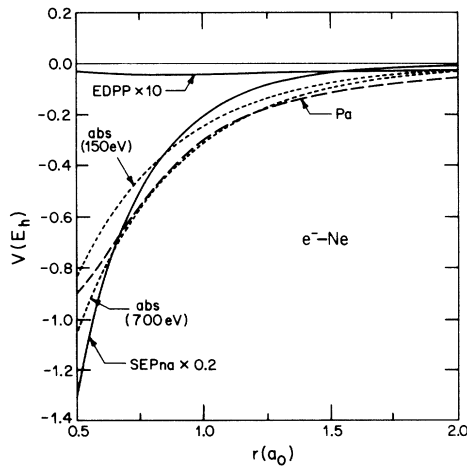


FIG. 1. Components of the interaction potential as functions of the distance of the scattering electron from the nucleus. The static-exchange-plus-nonadiabatic-polarization (SEPna) potential and its polarization part, the energy-dependent polarization potential (EDPP), are shown for an impact energy of 150 eV. The absorption (abs) potential is shown for both 150 and 700 eV impact energy, and the energy-independent adiabatic polarization (Pa) potential is also shown. The SEPna and EDPP potentials were multiplied by 0.2 and 10 before plotting.

$$\frac{d\sigma_{\text{el}}}{d\Omega} = \frac{1}{4k^2} \left| \sum_l (2l+1)(S_l-1)P_l(\cos\theta) \right|^2, \quad (16)$$

$$\sigma_{\text{el}} = \frac{\pi}{k^2} \sum_l (2l+1) |S_l-1|^2 \quad (17)$$

$$= 2\pi \int d\theta \sin\theta \frac{d\sigma_{\text{el}}}{d\Omega}, \quad (18)$$

$$\sigma_{\text{abs}} = \frac{\pi}{k^2} \sum_l (2l+1)(1-|S_l|^2), \quad (19)$$

$$\sigma_{\text{tot}} = \frac{2\pi}{k^2} \sum_l (2l+1)(1-\text{Re}S_l), \quad (20)$$

$$= \sigma_{\text{el}} + \sigma_{\text{abs}}, \quad (21)$$

$$\sigma_{\text{el}}^m = 2\pi \int d\theta \sin\theta (1-\cos\theta) \frac{d\sigma_{\text{el}}}{d\Omega}, \quad (22)$$

$$S_l = \exp(2i\eta_l), \quad (23)$$

where $d\sigma_{\text{el}}/d\Omega$ is the elastic differential cross section; θ is the scattering angle; σ_{el} , σ_{abs} , and σ_{tot} are the integral elastic, absorption, and total cross sections, respectively; σ_{el}^m is the elastic momentum-transfer cross section; and S_l is a diagonal element of the scattering matrix for orbital angular quantum number l . In the computation of differential cross sections for the MEP method the small- l contributions ($l \leq l_{(1)}$) were calculated as described above and augmented by asymptotic polarized Born phase shifts for large l ($l_{(1)} \leq l \leq l_{(2)}$). The asymptotic polarized Born approximation (APB) is the first Born approximation for the first term of the large- r expansion of the APP. This yields¹⁷

$$\eta_l = \tan^{-1} \frac{\pi\alpha_0 k^2}{(2l+3)(2l+1)(2l-1)}. \quad (24)$$

For each energy, $l_{(1)}$ and $l_{(2)}$ were chosen large enough so that differential cross sections were converged with respect to increasing either of them. The final values are given in Table II. For the optical-potential calculations, we included phase shifts for $l \leq l_{\text{max}}$ for the calculations with the

TABLE II. Angular momenta limits for differential cross sections using the present MEP method.

E (eV)	$l_{(1)}$	$l_{(2)}$	l_{max}	l'_{max}
150	62	120	34	43
200	71	130	36	49
400	87	150	30	67
700	107	260	29	100

EDPP polarization potential and for $l \leq l'_{\max}$ for the calculations with $V^{\text{Pa}}(r)$ where l_{\max} and l'_{\max} were chosen large enough so that a relative convergence of 10^{-6} was obtained in the calculation of elastic cross section and the absorption cross section. For the optical-potential calculations with no real polarization potential we used $l \leq l_{\max}$. The final values at all energies are given in Table II. To test the adequacy of these values of l_{\max} we repeated the MEP calculations with $l_{(2)}$ reduced to l_{\max} . We found that $d\sigma/d\Omega$ at 0° , where it is most sensitive, was reduced by less than 10% at all energies by this choice, and the integral and momentum-transfer cross sections were converged to more than three significant figures. Thus l_{\max} was judged adequate.

For comparison with the above results we also made calculations with the real $V^{\text{SEPa}}(r, E)$ potential. For these calculations we used numerically computed phase shifts for $l \leq l'_{\max}$ and augmented them with APB phase shifts for $(l'_{\max} + 1) \leq l \leq l_{(2)}$.

IV. RESULTS

Some of the calculated phase shifts are presented in Tables III and IV. The partial-wave contributions to the elastic and absorption cross sections in the MEP and SEPnaA models are presented in Table V. Table VI gives the total elastic cross section, the elastic momentum transfer cross section, the absorption cross section, and the total cross section obtained by all the methods studied here; the present results are compared here to previous experimental^{18–24} and theoretical^{25–29} values. Table VII contains the MEP values of the differential cross sections at four energies. Figures 2–5 and Table VIII compare the present calculations of the differential cross sections by the MEP, SEPa, and optical-potential methods to various experimental^{18, 19, 23, 30, 31} measurements and to the calculations of Byron and Joachain²⁵ and McCarthy *et al.*²⁶

V. DISCUSSION

A. Phase shifts

At high energy the adiabatic model (SEPa) should overestimate the polarization effect and thus yield phase shifts that are too high, corresponding to a polarization potential that is too attractive. Since accurate phase shifts are not

known for high-energy e^- -Ne scattering, we will treat the SEPa phase shifts as approximate upper bounds and the SE phase shifts as approximate lower bounds, and we will study the variations of the phase shifts of the other models with respect to these physical limits. The MEP and SEPnaA phase shifts are complex, and we will compare their real parts to the SEPa values. Table III shows that these phase shifts are less than SEPa values for all l and at all energies. Table III also shows that the SEPna phase shifts are considerably less than the SEPa values, showing that the EDPP model predicts large effects of nonadiabaticity. In fact the evidence of our previous study of the EDPP as applied to e^- -He scattering is that the EDPP overestimates the nonadiabaticity at high E and thus underestimates the attractiveness of the polarization contribution at high energy.⁴ We will return to this point when we compare the SEA, SEPnaA, and SEPaA cross sections to experiment. Our previous study of the MEP based on perturbation-theory adiabatic polarization potentials for e^- -He scattering also showed that δ_l (MEP) was usually not less than δ_l (SEPa); this violated our interpretation that the MEP includes the nonadiabatic effects in a natural way. The present application of the MEP based on variational adiabatic polarization potentials for e^- -Ne, however, does generally lead to $\delta_l(\text{MEP}) < \delta_l(\text{SEPa})$ for low l ; there is only one exception in Table III. This is more satisfactory. However, Table IV shows that at high l at 150 eV, $\delta_l(\text{MEP}) > \delta_l(\text{SEPa})$. This indicates that the effective optical potential implied by nonadiabatic calculations involving the MEP model is more attractive than $V^{\text{Pa}}(r)$ at large r , even though, as shown by Eq. (7), when the MEP coupled-channels equations are solved in the second-order adiabatic approximation, they do reduce to the correct adiabatic limit. In the next three paragraphs we examine some of the trends in the phase shifts more quantitatively.

The s -wave SEPna phase shifts at 150, 200, 400, and 700 eV are, respectively, 27%, 36%, 4%, and 4% lower than the SEPa values. Since for s -wave scattering there is no centrifugal potential, the incident electron experiences the short-range forces as fully as possible. For higher partial waves the centrifugal potential keeps the incident electron farther from the origin and hence the long-range polarization forces become more important. But even in the case of p and d waves there is a considerable decrease in the values of SEPna phase shifts as compared to the SEPa values. The percentage

TABLE III. Phase shifts for selected l values for various methods for low l and $l = 10$.

E (eV)	l	Phase shift (rad, mod π)				
		SE	SEPa ^a	SEPna ^b	MEP	SEPnaA
150	0	0.499	0.688	0.502	$0.601 + i0.141$	$0.505 + i0.187$
	1	1.932	2.161	1.936	$1.068 + i0.192$	$1.943 + i0.235$
	2	0.683	0.913	0.687	$0.859 + i0.176$	$0.681 + i0.178$
	6	0.014	0.045	0.017	$0.043 + i0.017$	$0.016 + i0.011$
	10	0.001	0.009	0.002	$0.011 + i0.004$	$0.002 + i0.001$
200	0	0.298	0.471	0.300	$0.373 + i0.122$	$0.303 + i0.207$
	1	1.843	2.050	1.846	$1.198 + i0.161$	$1.852 + i0.259$
	2	0.747	0.927	0.750	$0.874 + i0.167$	$0.746 + i0.205$
	6	0.024	0.061	0.026	$0.052 + i0.022$	$0.026 + i0.019$
	10	0.001	0.013	0.002	$0.013 + i0.006$	$0.002 + i0.002$
400	0	2.958	3.096	2.959	$2.993 + i0.080$	$2.961 + i0.199$
	1	1.635	1.792	1.636	$1.464 + i0.098$	$1.640 + i0.235$
	2	0.840	1.005	0.841	$0.888 + i0.106$	$0.840 + i0.203$
	6	0.068	0.172	0.069	$0.088 + i0.028$	$0.068 + i0.042$
	10	0.007	0.026	0.008	$0.018 + i0.011$	$0.008 + i0.009$
700	0	2.578	2.690	2.578	$0.545 + i0.053$	$2.580 + i0.152$
	1	1.470	1.594	1.470	$1.491 + i0.062$	$1.472 + i0.172$
	2	0.857	0.985	0.858	$0.879 + i0.065$	$0.858 + i0.154$
	6	0.123	0.181	0.123	$0.137 + i0.027$	$0.123 + i0.052$
	10	0.021	0.047	0.021	$0.029 + i0.013$	$0.021 + i0.017$

^a $V^{SEPa}(r, E) = V^{SE}(r, E) + V^{Pa}(r)$.

^b $V^{SEPna}(r, E) = V^{SE}(r, E) + V^{Pna}(r, E)$.

decrease is largest at 150 eV and least at 700 eV. At the higher energies the EDPP phase shifts do tend toward the SE values as expected, and at 700 eV the difference is negligible. Even at 150 eV the SE phase shifts are very similar to the SEPna ones for lower partial waves, but for higher partial

waves the SE phase shifts are too small. This is expected because the SE potential is short in range, and higher partial waves are more sensitive to long-range polarization effects.

Comparing the real parts of the MEP and SEPnaA phase shifts to each other, we see that δ_l ob-

TABLE IV. Phase shifts for selected l values for various methods for high l .

E (eV)	l	Phase shift (rad, mod π)			
		SE	MEP	SEPa	APB
150	15	9.573(-6)	$3.994(-3) + i6.644(-4)$	2.828(-3)	2.754(-3)
	20	1.595(-6)	$1.853(-3) + i1.443(-4)$	1.198(-3)	1.188(-3)
	25	1.853(-6)	$1.102(-3) + i3.794(-5)$	6.240(-4)	6.169(-4)
	30	1.988(-6)	$6.203(-4) + i1.044(-5)$	3.649(-4)	3.604(-4)
400	15	4.937(-4)	$5.886(-3) + i4.133(-3)$	7.772(-3)	7.344(-3)
	20	4.267(-5)	$3.062(-3) + i1.741(-3)$	3.286(-3)	3.169(-3)
	25	1.080(-5)	$1.845(-3) + i8.100(-4)$	1.693(-3)	1.645(-3)
	30	2.201(-6)	$1.200(-3) + i4.054(-4)$	9.848(-4)	9.610(-4)

tained by the SEPnaA method decreases most rapidly with increasing l . Furthermore the SEPnaA values of δ_l are very similar to the SEPna phase shifts. These facts indicate that the real part of the phase shifts is not very sensitive to the presence of the absorption potential (a result we also found using a different kind of absorption potential for e -He),³² and they are consistent with the EDPP underestimating the effect of polarization at high energy, as discussed above.

Now consider the variations in the imaginary part of the phase shift as predicted by the MEP and SEPnaA methods. Both the models yield much smaller γ_l as compared to δ_l , and the γ_l obtained by the SEPnaA method decreases more rapidly with l compared to the MEP values. However at all energies for small l values the γ_l values predicted by the SEPnaA model are larger than the MEP values. Eventually at larger l the MEP phase shifts become larger than the SEPnaA values. This means that the absorption potential "implied" by the MEP is longer in range than $V^A(r,E)$ of Green *et al.*

B. Elastic scattering

Figures 2–4 show that the MEP model yields excellent agreement with the experimental elastic differential cross sections at 150–700 eV. At 150 eV the MEP $d\sigma/d\Omega$ agrees with the experimental results within experimental error for $\theta \lesssim 40^\circ$ and for $\theta = 70^\circ$ – 100° ; at 50° , 60° , and 110° , it is about 20% below the experimental results of Gupta and Rees, and at 120° – 150° it is about 35% below their experimental result. The trend is similar at 200 eV in that agreement is again excellent at small θ and $d\sigma_{el}/d\Omega$ is underestimated at larger θ . At this energy though the difference from the average of the experimental results is 7%, 27%, 17%, 25%, and 41% at 30° , 60° , 90° , 120° , and 150° , respectively. At 400 eV one again finds some small underestimates at middle angles, but the agreement of theory and experiment is more uniform than in the other cases; at this energy the differences from the average or only available experimental results are only 0.3%, 8%, 9%, 5%, and 3% at 30° , 60° , 90° , 130° , and 160° , respectively. We can summarize these comparisons of the MEP $d\sigma_{el}/d\Omega$ to experiment as extremely encouraging.

Figures 3 and 4 also show that the SEPnaA calculations and the eikonal optical model of Byron and Joachain are about as accurate as the MEP

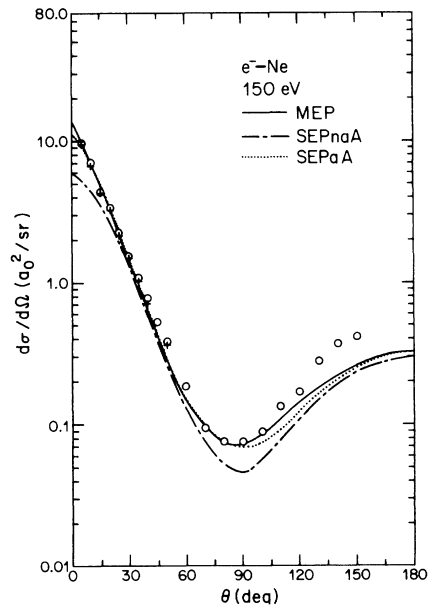


FIG. 2. Differential cross sections at 150-eV impact energy as functions of scattering angle. The theoretical results calculated here are shown as solid, long-dash—short-dash, and dotted curves as indicated in the figure. The experimental results of Gupta and Rees are shown as circles and those of Jensen *et al.* are shown as crosses.

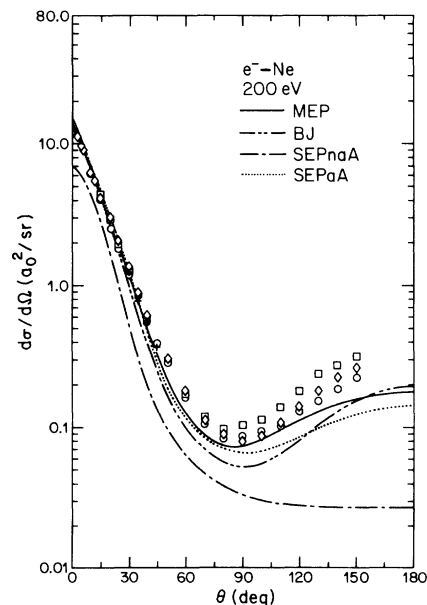


FIG. 3. Same as Fig. 2 except for 200 eV and three additional sets of differential cross sections are also included. The calculations of Byron and Joachain are shown as a long-dash—double-short-dash curve, the experimental results of Williams and Crowe are shown as squares, and those of Dubois and Rudd are shown as diamonds.

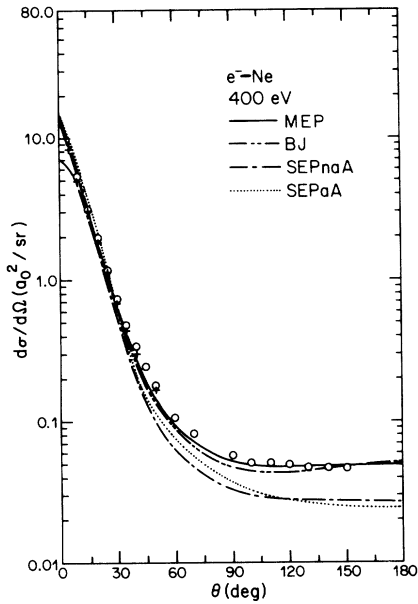


FIG. 4. Same as Fig. 3 except for 400 eV and only two sets of experimental results are available at this energy: those of Gupta and Rees are shown as circles and those of Jensen *et al.* are shown as crosses.

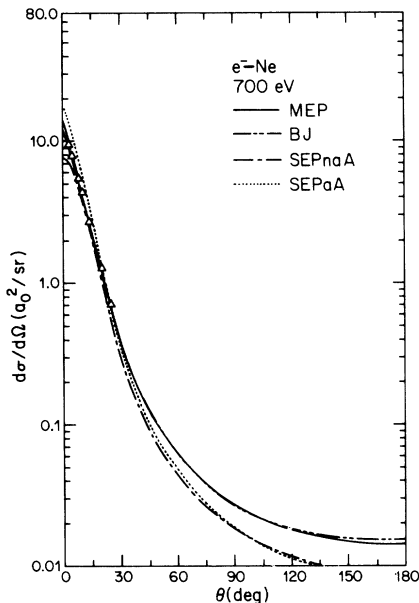


FIG. 5. Differential cross sections at 700-eV impact energy as functions of scattering angle. The experimental data of Bromberg are shown as triangles. Three sets of calculated values from the present work and the calculations of Byron and Joachain are shown as curves as indicated in the legend within the figure. The SEPna and SEPpA curves go off scale at the bottom; their values at 180° are $8.87 \times 10^{-3} a_0^2/\text{sr}$ and $8.54 \times 10^{-3} a_0^2/\text{sr}$, respectively.

model at low scattering angles but are uniformly less accurate than the MEP calculations at large θ . The SEPnaA model is in turn less accurate than the SEPpA model.

Table VI shows that the MEP model and the SEPpA model both predict accurate integral elastic cross sections and that the SEPnaA calculations systematically underestimate the integral elastic cross sections. These trends are consistent with those seen less quantitatively in Figs. 2–5. Since the MEP model predicts such accurate differential cross sections as well as integral cross sections, we conclude that the dependence of the partial cross sections on l is probably accurate. Tables III and V then indicate that the errors in the SEPnaA calculations are more important at high l than at low l , and that the SEPnaA calculations underestimate the high- l elastic scattering. This confirms that a large part of the fault in the SEPnaA calculations is that the EDPP is too weak (recall that Green *et al.* used an even weaker real polarization potential, i.e., zero). Table VI shows that indeed the EDPP used here for the real polarization potential does have only a small effect at these high energies, i.e., the SEPnaA results are very similar to the SEA results. The success of the SEPpA calculations is intriguing since there is little or no justification for using the APP at such high energies. We recall that our previous work on electron-He scattering also indicated that the EDPP is too weak at high energy.⁴ But there is no generally accepted better model for an energy-dependent real-polarization potential at high energy so it will be hard to improve on the SEPpA model using this kind of approach. The difficulty of modeling the energy dependence of the real-polarization potential, i.e., of modeling the energy dependence of nonadiabatic charge-polarization effects, is a central issue in the present study because it was the original motivation for developing the MEP. The MEP starts with the energy-independent APP and models nonadiabaticity in a very dynamical way, i.e., by embedding the APP in an effective coupled-channels problem. As we have just seen, this approach to nonadiabatic effects appears to be quite successful.

The excellent agreement of cross sections calculated using the MEP theory gives us confidence in trying to analyze the partial-wave contribution to elastic cross sections. Table V shows that according to the MEP and SEPnaA methods, p and d waves make the maximum contributions to the elastic cross sections at these energies. In particu-

TABLE V. Partial-wave contributions to the elastic and absorption cross sections (a_0^2) at impact energies 150–700 eV.

E (eV)	l	Elastic		Absorption	
		MEP	SEPnaA	MEP	SEPnaA
150	0	2.92(−1)	2.12(−1)	1.23(−1)	1.50(−1)
	1	1.87	1.96	4.59(−1)	5.27(−1)
	2	2.43	1.71	7.20(−1)	7.26(−1)
	3	7.24(−1)	4.06(−1)	5.16(−1)	5.42(−1)
	4	2.06(−1)	8.93(−2)	3.89(−1)	3.65(−1)
	5	7.21(−2)	2.12(−2)	3.05(−1)	2.40(−1)
	6	3.07(−2)	5.58(−3)	2.39(−1)	1.55(−1)
	≥ 7	4.03(−2)	2.57(−3)	8.21(−1)	2.56(−1)
200	0	9.91(−2)	7.48(−2)	8.27(−2)	1.20(−1)
	1	1.66	1.51	3.05(−1)	4.14(−1)
	2	1.89	1.43	5.20(−1)	5.98(−1)
	3	6.96(−1)	4.55(−1)	4.23(−1)	5.22(−1)
	4	2.20(−1)	1.26(−1)	3.34(−1)	3.94(−1)
	5	7.94(−2)	3.58(−2)	2.75(−1)	2.84(−1)
	6	3.36(−2)	1.08(−2)	2.29(−1)	1.99(−1)
	≥ 7	4.36(−2)	5.60(−3)	1.06	4.07(−1)
400	0	1.03(−2)	2.08(−2)	2.92(−2)	5.87(−2)
	1	1.05	8.43(−1)	1.04(−1)	1.95(−1)
	2	1.06	8.50(−1)	1.85(−1)	2.97(−1)
	3	5.51(−1)	4.40(−1)	2.03(−1)	3.22(−1)
	4	2.40(−1)	1.90(−1)	1.83(−1)	3.00(−1)
	5	1.01(−1)	7.89(−2)	1.61(−1)	2.60(−1)
	6	4.49(−2)	3.29(−2)	1.45(−1)	2.15(−1)
	≥ 8	2.14(−2)	1.40(−2)	1.31(−1)	1.73(−1)
700	0	5.97(−2)	5.54(−2)	1.17(−2)	2.78(−2)
	1	6.46(−1)	5.30(−1)	4.01(−2)	9.09(−2)
	2	6.41(−1)	5.35(−1)	6.98(−2)	1.40(−1)
	3	4.04(−1)	3.45(−1)	8.88(−2)	1.65(−1)
	4	2.21(−1)	1.91(−1)	9.30(−2)	1.71(−1)
	5	1.14(−1)	9.96(−2)	8.86(−2)	1.63(−1)
	6	5.82(−2)	5.08(−2)	8.20(−2)	1.49(−1)
	7	2.99(−2)	2.58(−2)	7.63(−2)	1.32(−1)
	8	1.58(−2)	1.32(−2)	7.16(−2)	1.14(−1)
	9	8.71(−3)	6.85(−3)	6.73(−2)	9.72(−2)
	≥ 10	1.59(−2)	7.87(−3)	9.34(−1)	4.34(−1)

lar the sum of the p - and d -wave contributions accounts for 76% of the MEP σ_{el} at 150 eV, 75% at 200 eV, 68% at 400 eV, and 58% at 700 eV. In contrast, in the SEPnaA model these two partial waves combine to give 65% of σ_{el} at 150 eV, 62% at 200 eV, 41% at 400 eV, and 48% at 700 eV. These values are less reliable since the SEPnaA model seems to yield too little forward scattering at all energies.

It is somewhat surprising that the SEPnaA model works so well in predicting the elastic cross sections at such high energy since the adiabatic polarization potential is generally regarded as too attractive at all energies, and this should be especially true at high energy. However, the adiabatic polarization model is usually applied without an absorption potential, and one would draw different conclusions about its validity when $V^A(r, E)$ is neglect-

TABLE VI. Integral and momentum transfer cross sections (a_0^2) at impact energies 150–700 eV.

E (eV)	150				200				400				700				
	σ_{el}	σ_{el}^m	σ_{abs}	σ_{tot}													
Experiment																	
Bromberg ^a					4.96				3.21								2.21
Gupta and Rees ^b	6.37	3.15			5.00	2.10			3.30	0.88							
Dubois and Rudd ^c					5.40	2.30											
Jansen <i>et al.</i> ^d	6.03				5.04				3.21								
deHeer <i>et al.</i> ^e	6.20		3.05	9.25	4.99		2.99	8.00	3.22		2.30	5.51	2.21		1.67	3.88	
Wagenaar and deHeer ^f				9.50				8.29				5.65				3.95	
Kauppila <i>et al.</i> ^g				9.02				7.98				5.47				3.90	
Theory																	
First Born ^h					12.3				6.44								4.25
Dewangen and Walters ^h					5.50		4.27	9.77	3.36		2.99	6.35	2.61		2.35	4.96	
Jhanwar <i>et al.</i> ⁱ	8.72		0.00	8.72	6.26		0.00	6.26	3.20		0.00	3.20	2.08		0.00	2.08	
McCarthy <i>et al.</i> ^j	5.82	2.91	2.99	8.81	4.87	2.06	2.97	7.84	3.26	0.88	2.28	5.54					
Byron and Joachain ^k					4.39	1.41	5.26	9.64	2.94	0.77	3.35	6.29	2.12	0.41	2.28	5.66	
Fon and Berrington ^l	6.31	3.72			5.17	2.70											
SE	6.04	3.93	0.00	6.04	5.07	2.83	0.00	5.07	3.31	1.14	0.00	3.31	2.31	0.51	0.00	2.31	
SEPa	7.71	4.37	0.00	7.71	6.55	3.10	0.00	6.55	4.31	1.22	0.00	4.31	2.46	0.70	0.00	2.46	
SEA	4.38	1.88	2.95	7.33	3.60	1.24	2.92	6.52	2.47	0.53	2.38	4.85	1.86	0.29	1.68	3.54	
SEPnaA	4.41	1.88	2.96	7.37	3.65	1.26	2.94	6.59	2.48	0.53	2.39	4.87	1.86	0.29	1.68	3.55	
SEPaA	5.74	2.17	3.03	8.76	4.79	1.43	2.99	7.78	3.26	0.58	2.41	5.67	2.44	0.31	1.70	4.14	
MEP	5.67	2.26	3.57	9.24	4.72	1.68	3.23	7.95	3.11	0.81	2.29	5.40	2.21	0.31	1.62	3.84	

^aReference 18.

^bReference 19. The values of σ_{el} and σ_{el}^m reported by Gupta and Rees are inconsistent with their $d\sigma_{el}/d\Omega$ from which they computed them. We repeated their calculation using Eqs. (18) and (22) to obtain the values tabulated here. We note that this reintegration brings their values of σ_{el} into better agreement with those of other workers.

^cReference 23. The value of σ_{el}^m was obtained by extrapolation and integration of their reported differential cross section. The extrapolation was guided by the present SEPnaA results.

^dReference 20.

^eReference 21.

^fReference 22.

^gReference 24.

^hReference 27.

ⁱReference 28 (values at 700 eV are interpolated).

^jReference 26. These authors report only $d\sigma_{el}/d\Omega$ and σ_{abs} . We corrected the units on their σ_{abs} and calculated the other quantities tabulated here by Eqs. (18), (21), and (22).

^kReference 25. These authors report only $d\sigma_{el}/d\Omega$ and σ_{tot} . We calculated the other quantities tabulated here by Eqs. (18), (21), and (22).

^lReference 29. These authors did not report σ_{abs} or σ_{tot} .

ed. Table VI shows that the SEPa model overestimates σ_{el} and σ_{el}^m at all energies, with the percent overestimate higher for the latter. Table VIII shows that neglecting the absorption part of the SEPaA model overestimates the elastic differential cross sections at all energies with the relative difference between the SEPa and SEPaA values being larger at larger scattering angles. These trends are consistent with the fact that the absorption part of the SEPaA potential absorbs flux from the elastic channel, and, being more short range than the real part of the potential, its greatest relative

effect is at small r and hence large θ . In summary, these results show that even for elastic scattering, it is important to include the effect of absorption to calculate accurate cross sections and to draw valid conclusions about the quantitative adequacy or inadequacy of various model potentials.

C. Inelastic and total scattering

Table VI shows that the inelastic cross sections predicted by the optical-potential calculations are much less sensitive than the elastic cross sections

TABLE VII. Differential cross sections (in a_0^2/sr) for elastic scattering of electrons by neon in the energy range 150–700 eV, as obtained from the present MEP method.

θ (deg)	E (eV)			
	150	200	400	700
0	13.8	14.0	13.8	13.9
5	10.0	9.60	8.39	7.47
10	7.04	6.44	5.12	4.29
15	4.87	5.48	3.12	2.40
20	3.31	4.27	1.86	1.30
25	2.22	1.81	1.11	3.19(–1)
30	1.47	1.16	6.64(–1)	4.19(–1)
40	6.40(–1)	4.84(–1)	2.73(–1)	1.77(–1)
50	2.92(–1)	2.24(–1)	1.44(–1)	9.69(–2)
60	1.51(–1)	1.25(–1)	9.44(–2)	6.24(–2)
70	9.44(–2)	8.68(–2)	7.11(–2)	4.43(–2)
80	7.38(–2)	7.37(–2)	5.86(–2)	3.36(–2)
90	7.21(–2)	7.38(–2)	5.16(–2)	2.70(–2)
100	8.41(–2)	8.21(–2)	4.78(–2)	2.28(–2)
110	1.07(–1)	9.54(–2)	4.60(–2)	1.99(–2)
120	1.40(–1)	1.11(–1)	4.55(–2)	1.80(–2)
140	2.20(–1)	1.44(–1)	4.62(–2)	1.53(–2)
160	2.92(–1)	1.68(–2)	4.75(–2)	1.46(–2)
180	3.22(–1)	1.76(–1)	4.78(–2)	1.43(–2)

to the real-polarization potential. Furthermore Tables III and V show that the optical-potential calculations, with the absorption potential of Green *et al.*,⁸ predict more inelasticity than the MEP calculations do at small l but less at high l . It is hard to judge which model is more accurate for this feature so it will be interesting to compare the results in these tables to any future theoretical treatments of this problem. Table VI shows that the optical potential σ_{abs} agree with experiment at each energy, but that is simply a consequence of Green *et al.* having successfully adjusted their parameters

to achieve this. The comparison of the MEP calculations to the experimental σ_{abs} is more instructive since these calculations contain no adjustable parameters. The comparison in Table VI shows that the present calculations agree with experiment within 17%, 8%, 0.4%, and 3% at 150, 200, 400, and 700 eV. We conclude that the present MEP performs excellently for this problem. In fact, since the MEP model predicts the energy dependence of σ_{abs} so accurately with no parameters adjusted to experiment, one is tempted to put some trust in the l dependence for a general energy. If

TABLE VIII. Differential cross sections (a_0^2/sr) for elastic scattering of electrons from neon at impact energies 150 and 400 eV.

θ (deg)	150					400				
	SEPa	SEPaA	MEP	McCarthy <i>et al.</i> ^a	Expt. ^b	SEPa	SEPaA	MEP	McCarthy <i>et al.</i> ^a	Expt. ^b
10	7.28	7.19	7.04	6.51	7.11	6.80	6.62	5.12	5.75	5.39
30	1.83	1.55	1.47	1.42	1.54	0.911	0.611	0.664	0.578	0.729
60	0.274	0.152	0.151	0.155	0.183	0.155	0.0771	0.0944	0.0931	0.103
90	0.117	0.0689	0.0721	0.0532	0.058	0.0833	0.0314	0.0516	0.0555	0.057
120	0.251	0.123	0.140	0.171	0.169	0.0687	0.0280	0.0455	0.0534	0.048
140	0.0487	0.207	0.220	0.338	0.464	0.0667	0.0259	0.0462	0.0565	0.047
150	0.821	0.251	0.260	0.422	0.689	0.0663	0.0253	0.0469	0.0580	0.046

^aReference 26.

^bReference 19.

we accept this, then the discussion above of Tables III and V gives a constructive clue for improving the optical potential of Green *et al.*, namely, that the functional form should be given a longer range.

D. Comparison with other methods

The results of the MEP method studied here are compared in this section to the results obtained by previous workers.

The approach of McCarthy *et al.*²⁶ is a phenomenological one very similar to that adopted by Green *et al.*⁸ They used a static-exchange potential very similar to the one used here, but they used the hydrogenic adiabatic dipole approximation,³³ scaled to give the correct dipole polarizability of Ne, to obtain an approximate energy-independent $V^{\text{Pa}}(r)$. The absorption potential was taken to have the phenomenological form

$$V^{\text{abs}}(r, E) = \frac{-W(E)}{[E - V^{\text{SEPa}}(r, E)]^2} u_i^2(r), \quad (25)$$

where $u_i(r)/r$ is a valence orbital³⁴ and the strength parameter $W(E)$ was adjusted to give the correct absorption potential at all energies. Since σ_{abs} comes out right by adjustment, the test of their model is the accuracy of the predicted elastic cross sections. Tables VI and VIII show that these are actually slightly more accurate than those predicted by the SEP_aA model studied here. Thus this phenomenological approach has merit. In fact the elastic differential cross section calculated by McCarthy *et al.* is the most accurate theoretical value at all scattering angles at 150 eV, and it is in good agreement with experiment at 400 eV. The good agreement of their results with experiment even at medium and large scattering angle is reflected in their calculations of σ_{el}^m , which uniformly agree better than any other model with the experimentally measured values (see Table VI). It is interesting that the values of $d\sigma_{\text{el}}/d\Omega$ and σ_{el}^m predicted by the MEP model become increasingly accurate at higher energies, and at 400 eV the MEP differential cross section is more accurate than the McCarthy *et al.* one at all scattering angles even though the McCarthy *et al.* potential has a parameter adjusted to experiment but the MEP model does not.

We can also compare to results obtained by the eikonal optical theory which has been applied to electron-atom scattering by Byron, Joachain, and Vanderpoorten.^{25,35,36} This theory is based on

multiple-scattering expansion of the optical potential in terms of the full interaction between the atom and the incident electron. Exchange effects are included by the Mittleman-Watson exchange potential,³⁷ which has been tested elsewhere.³⁸ Polarization and absorption effects are included by seeking a local, spherically symmetric form for the effective potential such that the eikonal amplitude from this potential agrees through second order with the many-body Glauber amplitude. For the imaginary part of the potential this criterion yields an integral equation that can be solved for an absorption potential $V_G^{\text{abs}}(r, E)$. The resulting $V_G^{\text{abs}}(r, E)$, however, has an "incorrect" behavior at large r because the Glauber amplitude has serious defects for small scattering angles. This problem is corrected by taking the difference between the second-Born amplitude and the amplitude obtained in the Glauber approximation to second order and Fourier transforming the difference amplitude. This yields a correction potential $V^{\text{corr}}(r, E)$, which is added to $V_G^{\text{abs}}(r, E)$ to give the eikonal optical-absorption potential. The interested reader is referred to Refs. 25 and 36 for a discussion of the real part of the eikonal optical potential and for further details. Figures 3–5 and Table VI show that the eikonal optical model is almost as successful as the MEP model for elastic cross sections although it does seem to slightly underestimate them. However, it is much less successful than the MEP model for the absorption cross sections, which it systematically overestimates. Whereas the errors in the MEP values of σ_{abs} do not exceed 8% at 200–700 eV (see above), the Byron-Joachain calculations differ from the experimental σ_{abs} by 76–37% over this energy range.

Dewangen and Walters²⁷ applied a distorted-wave second-Born approximation to calculate σ_{el} and σ_{tot} at energies of 200 eV and higher. Their elastic cross sections are reasonably accurate, but their σ_{abs} cross sections are systematically too high by 30–43%.

Jhanwar *et al.*²⁸ applied a real effective potential of the SEP type. Since they neglect the absorption potential their method yields zero for σ_{abs} . This probably also explains why their calculations overestimate σ_{el} at 200 and 400 eV.

Fon and Berrington²⁹ performed R matrix calculations in which the ground-state wave function is coupled to a 1P pseudostate. These calculations are in excellent agreement with the experimental differential and integral elastic cross sections at both 150 and 200 eV.

VI. GENERAL CONCLUSION

The MEP model is very successful at predicting the integral and differential cross sections for elastic scattering and the absorption cross section for electron-neon collisions at 150–700 eV. In fact it is even more successful for this case than it was for electron-helium scattering,^{3,4} although it was quite successful in that case too. These studies show that the MEP approach deserves further study, and it should be considered a strong candidate for making predictive calculations on practical problems where no data is available for adjusting parameters and where a more rigorous calculation is prohibitively difficult.

ACKNOWLEDGMENTS

The authors are grateful to Dr. A. E. S. Green for a prepublication copy of Ref. 8. This work was supported in part by the National Science Foundation through Grant No. CHE80-25232.

APPENDIX

The leading energy-independent terms in the large- r polarization potential are³⁹

$$V^P(r) \underset{r \rightarrow \infty}{\sim} -\frac{\alpha_0}{2r^4} + \frac{3\beta}{r^6}, \quad (\text{A1})$$

where α_0 is the static dipole polarizability and β is the leading nonadiabatic coefficient. In the dipole approximation

$$\alpha_0 = 2 \sum_{n \neq 1} \frac{|z_{n1}|^2}{\omega_n} \quad (\text{A2})$$

and

$$\beta = \sum_{n \neq 1} \frac{|z_{n1}|^2}{\omega_n^2}, \quad (\text{A3})$$

where ω_n is the excitation energy of state n . If we make the average-energy approximation ($\omega_n = \omega$) we obtain

$$\alpha_0 = 2S/\omega \quad (\text{A4})$$

and

$$\beta = S/\omega^2, \quad (\text{A5})$$

where

$$S = \sum_{n \neq 1} |z_{n1}|^2. \quad (\text{A6})$$

Combining (A4) and (A5) yields a value for the average excitation energy

$$\omega = \alpha_0/2\beta. \quad (\text{A7})$$

For Ne, we take $\alpha_0 = 2.359a_0^3$ (Ref. 7) and $\beta = 1.27a_0^5$ (Ref. 39). Then (A7) yields $\omega = 0.9288E_n$.

¹B. H. Bransden and M. R. C. McDowell, Phys. Rep. C **30**, 207 (1977); **46**, 249 (1978).

²D. G. Truhlar, D. A. Dixon, R. A. Eades, F. A. Van-Catledge, and K. Onda, in *Electron-Molecule and Photon-Molecule Collisions*, edited by T. N. Rescigno, V. McKoy, and B. I. Schneider (Plenum, New York, 1979), p. 151; D. G. Truhlar, K. Onda, R. A. Eades, and D. A. Dixon, Int. J. Quantum Chem. Symp. **13**, 601 (1979); D. G. Truhlar, in *Chemical Applications of Atomic and Molecular Electrostatic Potentials*, edited by P. Politzer and D. G. Truhlar (Plenum, New York, 1981), p. 123.

³D. G. Truhlar and K. Onda, Phys. Lett. **76A**, 119 (1980).

⁴K. Onda and D. G. Truhlar, Phys. Rev. A **22**, 86 (1980).

⁵D. Thirumalai and D. G. Truhlar, J. Chem. Phys. **76**, 385 (1982).

⁶A. Dalgarno and N. Lynn, Proc. Phys. Soc. London, Ser. A **70**, 223 (1957).

⁷C. H. Douglass, Jr., D. A. Weil, P. A. Charlier, R. A. Eades, D. G. Truhlar, and D. A. Dixon, in *Chemical Applications of Atomic and Molecular Electrostatic Potentials*, edited by P. Politzer and D. G. Truhlar (Plenum, New York, 1981), p. 173.

⁸A. E. S. Green, D. E. Rio, and T. Ueda, Phys. Rev. A **24**, 3010 (1981).

⁹T. G. Strand and R. A. Bonham, J. Chem. Phys. **40**, 1686 (1964).

¹⁰M. E. Riley and D. G. Truhlar, J. Chem. Phys. **63**, 2182 (1975).

¹¹M. A. Brandt and D. G. Truhlar, Chem. Phys. Lett. **23**, 48 (1973); R. T. Pack, J. Chem. Phys. **60**, 633 (1974); P. McGuire and D. J. Kouri, J. Chem. Phys. **60**, 2488 (1974); M. A. Brandt and D. G. Truhlar, Chem. Phys. **13**, 461 (1976).

¹²C. C. J. Roothaan, L. M. Sachs, and A. W. Weiss, Rev. Mod. Phys. **32**, 191 (1960).

¹³D. G. Truhlar, N. M. Harvey, K. Onda, and M. A. Brandt, in *Algorithms and Computer Codes for Atomic*

- and *Molecular Quantum Scattering Theory*, edited by L. Thomas (National Resource for Computation in Chemistry, Lawrence Berkeley Laboratory, Berkeley, Calif., 1979), Vol. I, p. 220.
- ¹⁴F. Calogero, *Variable Phase Approach to Potential Scattering* (Academic, New York, 1967), p. 11; M. A. Brandt, M. S. thesis, University of Minnesota, Minneapolis, 1975 (unpublished).
- ¹⁵L. D. Landau and E. M. Lifshitz, *Quantum Mechanics*, 2nd ed. (Pergamon, Oxford, 1965), pp. 542–543.
- ¹⁶A. E. S. Green, T. Sawada, and D. S. Saxon, *The Nuclear Independent Particle Model* (Academic, New York, 1968), Sec. 3.1.
- ¹⁷T. F. O'Malley, L. Spruch, and L. Rosenberg, *J. Math. Phys.* **2**, 491 (1961).
- ¹⁸J. P. Bromberg, *J. Chem. Phys.* **61**, 963 (1974).
- ¹⁹S. C. Gupta and J. A. Rees, *J. Phys. B* **8**, 419 (1975).
- ²⁰R. J. H. Jansen and F. J. deHeer, *J. Phys. B* **9**, 213 (1976).
- ²¹F. J. deHeer, R. J. H. Jansen, and W. Van der Kaay, *J. Phys. B* **12**, 979 (1979).
- ²²R. W. Wagenaar and F. J. deHeer, *J. Phys. B* **13**, 3855 (1980).
- ²³R. D. Dubois and M. E. Rudd, *J. Phys. B* **9**, 2659 (1976).
- ²⁴W. E. Kauppila, J. S. Stein, J. H. Smart, M. S. Dababneh, Y. K. Ho, J. P. Downing, and V. Pol, *Phys. Rev. A* **24**, 725 (1981).
- ²⁵F. W. Byron, Jr. and C. J. Joachain, *Phys. Rev. A* **15**, 128 (1977).
- ²⁶I. E. McCarthy, C. J. Noble, B. A. Philips, and A. D. Turnbull, *Phys. Rev. A* **15**, 2173 (1977).
- ²⁷D. P. Dewangen and H. R. J. Walters, *J. Phys. B* **10**, 637 (1977).
- ²⁸B. L. Jhanwar, S. P. Khare, and A. Kumar, *J. Phys. B* **11**, 887 (1978).
- ²⁹W. C. Fon and K. A. Berrington, *J. Phys. B* **14**, 323 (1981).
- ³⁰J. F. Williams and A. Crowe, *J. Phys. B* **8**, 2233 (1975).
- ³¹R. J. H. Jansen, F. J. deHeer, H. J. Luyken, B. van Wingerden, and H. J. Blaauw, *J. Phys. B* **9**, 185 (1976).
- ³²S. M. Valone, D. Thirumalai, and D. G. Truhlar, *Int. J. Quantum Chem. Symp.* **15**, 341 (1981).
- ³³A. Temkin and J. C. Lamkin, *Phys. Rev.* **121**, 788 (1961); R. J. Drachman and A. Temkin, *Case Stud. At. Coll. Phys.* **2**, 399 (1972).
- ³⁴C. Froese-Fischer, *At. Data* **4**, 301 (1972).
- ³⁵R. Vanderpoorten, *J. Phys. B* **8**, 926 (1975).
- ³⁶F. W. Byron, Jr. and C. J. Joachain, *Phys. Rep.* **34**, 233 (1977).
- ³⁷M. H. Mittleman and K. M. Watson, *Ann. Phys. (N.Y.)* **10**, 268 (1960).
- ³⁸M. E. Riley and D. G. Truhlar, *J. Chem. Phys.* **65**, 792 (1976).
- ³⁹C. J. Kleinman, Y. Hahn, and L. Spruch, *Phys. Rev.* **165**, 53 (1968).